Journal of Power Sources 232 (2013) 55–65

Contents lists available at SciVerse ScienceDirect

Journal of Power Sources

journal homepage: www.elsevier.com/locate/jpowsour

Synthesis of nanocrystalline lanthanum manganite with tailored particulate size and morphology using a novel spray pyrolysis technique for application as the functional solid oxide fuel cell cathode

Jayanta Mukhopadhyay, Himadri Sekhar Maiti [1], Rajendra Nath Basu*

Fuel Cell and Battery Division, CSIR-Central Glass and Ceramic Research Institute, Kolkata – 700 032, India

HIGHLIGHTS

- ► Spray pyrolysed nanocrystalline LSM possess tailored particulate size and morphology.
- ► Precalcined LSM nanoparticles used as seeding agent for in-situ particle growth.
- ► Tailored morphology of functional cathode results in lowest polarization (0.4 Ω-cm^2).
- ► Functional cathode enhances cell performance appreciably (3.2 A cm^{-2}, 0.7 V & 800 °C).
- ► Functional cathode also reduces cell ASR down to 0.109 Ω-cm^2 at 800 °C.

ARTICLE INFO

Article history:
Received 8 November 2012
Received in revised form
10 December 2012
Accepted 12 December 2012
Available online 11 January 2013

Keywords:
Solid oxide fuel cell cathode
Spray pyrolysis
Nanocrystalline lanthanum manganite
Particulate morphology
Cathode overpotential
Cell performance

ABSTRACT

Nanocrystalline strontium doped lanthanum manganite ($La_{0.65}Sr_{0.3}MnO_3$) having variable particulate sizes and morphology is synthesized by a novel spray pyrolysis (SP) technique for solid oxide fuel cell (SOFC) cathode. Precalcined nanopowders received from the first SP run are added as the seeding agent in the subsequent runs for their in-situ growth inside the reactor. The suitability of the nano and micro particulates having interconnected porosity are examined as cathode functional and current collection layers. Detailed physical, microstructural and bulk electrical characterizations of such nanopowders are studied. Cathode polarization behavior and the associated rate limiting steps are characterized using AC impedance spectroscopy in the symmetric cell configurations. The optimization of the cathode processing conditions has brought the interfacial polarization down to ~0.2 Ω-cm^2 and thereby increases the cell performance from 2.0 to 3.2 A.cm^{-2} (0.7 V, 800 °C). Such improvement in anode-supported SOFC is correlated with the cathode processing conditions, particulate size, morphology and cathode microstructure.

1. Introduction

The transition from electrolyte supported to electrode-supported designs has induced significant affirmative aspects in the development of solid oxide fuel cells (SOFCs). Electrode-supported cells are categorized into cathode and anode-supported cells. Between these two types, anode-supported cells having thin electrolyte (10–30 μm) can be operated at much lower temperatures of 600–800 °C [1]. The ohmic loss for such thin electrolyte is found to be negligible for the cell operating at 700–800 °C. The cathode polarization can be minimized by lowering the SOFC operating temperature [1]. Therefore, selection of appropriate cathode material is important to improve the cell performance [2]. Electrode kinetics is also found to be retarded upon reducing the cell operating temperature and thereby enhances the interfacial polarization resistance. This eventually affects the oxygen reduction reaction (ORR) at the cathode. High catalytic activity for oxygen reduction is maintained at the cathode for its effective performance as the oxygen reduction electrode [3]. In general, materials having mixed ionic and electronic conductivity (MIEC) reduce the cathode polarization related to the electrochemical reduction of oxidant [4,5]. The composite of Sr-substituted $LaMnO_3$ (LSM) and 8 mol% yittria stabilized zirconia (YSZ) is found to be the most widely used cathode for SOFC application [4]. While LSM–YSZ provides good performance at ~800 °C, the interfacial

* Corresponding author. Tel.: +91 33 2473 3469x3507; fax: +91 33 2473 0957.
E-mail addresses: rajenbasu54@gmail.com, rnbasu@cgcri.res.in (R.N. Basu).
[1] Present Address: Department of Ceramic Engineering, NIT, Rourkela 769008, Orissa, India.

0378-7753/$ – see front matter © 2013 Elsevier B.V. All rights reserved.
http://dx.doi.org/10.1016/j.jpowsour.2012.12.113

polarization at the cathode–electrolyte junction reduces rapidly with higher cell operating temperature. Inhomogeneous cathode microstructure within the cell also causes a non-uniform current distribution during cell operation that leads to variation of local current density at the cathode. This inhomogeneity results in further microstructural degradation with lower cell performance [4]. The inhomogeneous cathode microstructure is responsible for compositional changes by chemical reactions; grain growth and delamination at the cathode-electrolyte interface [6–8]. In addition, stability of the cathode-electrolyte interface plays an important role in minimizing the electrode polarization [9,10]. It is well known that, the formation of $La_2Zr_2O_7$ through high temperature interaction between $La_{1-x}Sr_xMnO_3$ and YSZ increases the cathode-electrolyte interface polarization resistance [2,11]. Several groups of researchers have studied the overpotential of LSM based cathode current collection layer and LSM–YSZ composite cathode reaction layer at temperatures $\geq$800 °C [12,13]. The interfacial resistance (R_i), measured at a definite temperature, is found to drop as the YSZ/LSM weight ratio is increased to ~1.0 [14]. Nanoporous cathodes are expected to exhibit a lower cathodic overpotential because of the availability of large effective surface area for electrocatalytic reactions. But such cathodes are generally vulnerable to degradation at high temperatures. Owing to such features, short-term performances of cells having such cathodes are superior compared to their long-term activity [15]. For better cell performance, nanocrystalline cathodes having significant catalytic activity with desired particulate sizes and morphologies are found to be the crucial [16]. Detailed investigation has been carried out on samarium strontium cobaltite (SSC) cathode system based on the control of particulate morphology and cathode microstructure and their effect on the electrochemical performance [17]. It is observed that, nanocrystalline cathode structures developed from nanopowders having mesoporosity induce higher rate of oxygen diffusion at cathode surface and hence reduce the polarization losses of the cathode layer [18,19]. Synthesis of the nanocrystalline cathodes have been studied by sol–gel, glycine-nitrate, impregnation, pulsed laser deposition or radio frequency (RF) sputtering etc. [20–24]. Spray pyrolysis (SP) is still considered to be one of the most effective methods for synthesizing nanocrystalline cathodes. The prime advantages of SP involve easier technique for synthesizing the multicomponent oxides in a single step according to the applicability, better homogeneity in nanoscale and up-scalability [25].

Under the present investigation, influence of particulate size and morphology of nanocrystalline $La_{0.65}Sr_{0.3}MnO_3$ (LSM)-based cathodes prepared by spray pyrolysis technique is studied in details. A unique approach is adopted using a novel low temperature spray pyrolysis technique for synthesizing nanopowders of LSM to be used for SOFC cathode functional layer (CFL) and cathode current collection layer (CCCL) application. Attempt has been made to add SP derived precalcined LSM nanopowders in the precursor solution as the seeding agent during subsequent runs of the pyrolysis. Use of such precalcined LSM powder as a seed material for in-situ growth inside the reactor during the pyrolysis reaction may lead to the formation of porous micro granules of LSM with different particulate morphology. A comprehensive effort is made to understand the material properties of such SP synthesized nano and micro LSM powders having different particulate size and morphology. Detailed electrical characterizations and polarization behaviors are studied using DC electrical conductivity and electrochemical impedance spectroscopy (EIS) measurements to correlate the polarizations of SP synthesized cathodes with the particulate size and morphology. Finally, electrochemical activity of the optimized cathode composition is studied in the form of current–voltage relationship for SOFC single cell. A clinical correlation is also described among cell performance, cathode particulate size, morphology and cell microstructure.

2. Experimental

2.1. Synthesis, preparation and characterization of LSM and LSM–YSZ cathode powders

For the preparation of Sr-doped lanthanum manganite ($La_{0.65}Sr_{0.3}MnO_3$) composition, lanthanum nitrate hexahydrate (Sisco Research Laboratory Pvt. Ltd., India, >99.0%), strontium nitrate (s. d. fine chem. Ltd., India, >99%), manganese (II) acetate tetra hydrate (E Merck India Limited, >99.5%) and citric acid monohydrate (E Merck India Limited, Mumbai, India, >99.5%) were used as the precursor materials. Stock solutions of lanthanum nitrate hexahydrate and strontium nitrate were prepared having different molar concentrations viz. 0.2 M, 0.5 M, 0.75 M and 1.0 M and were used as the nitrate precursor solutions. Stoichiometric amount of the metal nitrate solutions (N) and the acetate salt of manganese were mixed together to form the precursor salt solution. Citric acid monohydrate (C) was used both as chelating agent and fuel (in the combustion reaction) and was added to the above precursor salt solution so as to have a C/N ratio in the range between 0.5 and 0.6. The precursor solution was sprayed into the reaction zone of an indigenously made pyrolyser using a peristaltic pump and the two fluid nozzle assembly. The inlet temperature of the spray unit was maintained at 400 °C. The ashes generated as a result of the auto-combustion reaction was collected in cyclonic separators as coarser and finer fractions respectively. Gaseous reaction products such as NO_x, CO_2 etc. were scrubbed out by passing out the same through a scrubber attached at one end of the system. A schematic of the spray pyrolysing set up is given in Fig. 1. In order to have sufficient particulate growth during the pyrolysis reaction, batches were also formulated with a definite amount of addition of precalcined ashes derived out of the previous pyrolysis into the precursor solution as the seeding agent. The as-synthesized powders received from the first run of 0.25 M solution was added as seeding agents to the precursor solution having concentration range from 0.25 M to1.0 M of the precursor solutions for the subsequent runs. The particulate loading were kept constant at 25 wt % of the theoretical yield of 0.25 M precursor solution. Various LSM batch formulations thus prepared under the present investigation are given in Table 1. The synthesized powders were calcined at a temperature of 950 °C for 4 h. The phase identification of the as-prepared and the calcined LSM powders was confirmed by X-ray powder diffraction (XRD) data collected at a scan rate of 2° min^{-1} from X-ray diffractometer (Philips X'pert, PANalytical, Netherlands) with Cu-Kα radiation. Rietveld refinement of the diffraction data was carried out by PANalytical X'Pert High Score software using a pseudovoight function. The morphologies of the SP powders prepared under various synthesis conditions were examined by field emission scanning electron microscopy (FESEM – Gemini Supra 35, Zeiss). Brunauer–Emmett–Teller (BET) surface area of the powders was also characterized using a surface analyzer (Nova 4000 E, Quantachrome, USA). In addition, the particle size of the synthesized powders was also determined from the results of BET surface area. Among the synthesized compositions mentioned in Table 1, optimized LSM powders were selected based on particle size and morphology, to be used as cathode functional layer (CFL) and cathode current collection layer (CCCL) in the single cells. The primary selection criterion of LSM for CFL was, to have close proximity with that of particle size of 8YSZ (Tosho Corporation, Japan; d_{50} ~ 0.2 μm) having nanocrystallinity and interconnected porosity. Cathode functional layer was prepared upon mixing the optimized LSM with 8 YSZ for 4 h in a planetary mill (Fritsch,

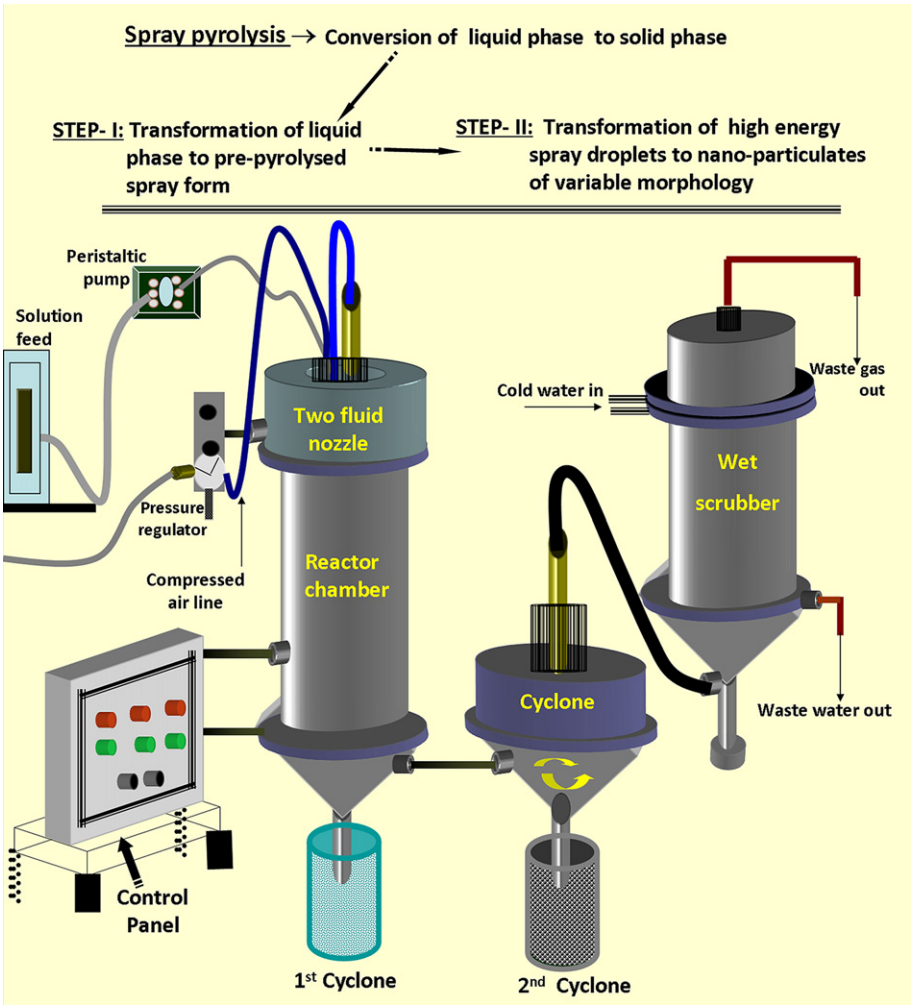

Fig. 1. Schematic of spray pyrolysis set up.

Germany) having rotational speed of 250 rpm with an equal weight ratio of 1:1 using isopropanaol as the medium. Unlike CFL, LSM powder to be used as cathode current collection layer (CCCL) needs to be microporous larger particulates containing several primary nanoparticulates within and also having interconnected pores. Such interconnected microstructure is expected to minimize the diffusion polarization at the cathode/oxidant interface and therefore could be effective enough to collect the cathode current after proper heat treatment. It is expected that the particulates synthesized with seeding of nanocrystalline precalcined ashes may be effective for such use and hence optimized composition was selected among LS-1.1 to 1.4 (Table 1) for CCCL application.

Table 1
Batch formulation, surface area and particle size of SP synthesized cathode powders.

Concentration of precursor solution (M)	Precalcined ash used for solid loading (% of precalcined ashes of precursor concentration -M)	Experimental sample ID	Surface area of the synthesized cathode powders ($m^2\ g^{-1}$)	Particulate sizes of synthesized cathode powders (μm)	Suitability of application in SOFC cathode
SP powders without solid loading					
0.25	–	LS-1	5.546	0.18	–
0.5	–	LS-2	4.159	0.24	Cathode functional layer (CFL)
0.75	–	LS-3	3.565	0.28	–
1.0	–	LS-4	3.119	0.32	–
SP powders with solid loading					
0.25	25% ash of 0.25 (M) precursor	LS-1.1	1.854	0.54	–
0.5	25% ash of 0.25 (M) precursor	LS-1.2	0.876	1.14	–
0.75	25% ash of 0.25 (M) precursor	LS-1.3	0.233	4.27	–
1.0	25% ash of 0.25 (M) precursor	LS-1.4	0.208	4.80	Cathode current collection layer (CCCL)

2.2. Electrical characterizations of SP synthesized cathode powders

For determination of bulk electrical properties of LSM powders suitable for the use as cathode functional and current collection layers, the calcined powders were compacted in the form of rectangular bars using a uniaxial pressure of 170 MPa. The green compacts were sintered in air for 4 h at various temperatures in the range of 950–1150 °C. Sintered samples were measured for open porosity using Archimedes principle. DC electrical resistances of the sintered bar samples, thus obtained, were measured by 4-probe technique using an 8½ digit multimeter (Keithley, 2002). The corresponding conductivity values in temperature range 500–800 °C are then calculated using the formula,

$$\sigma = \frac{L}{Rbt} \quad (1)$$

where, σ is the conductivity, 'R' is the resistance of the samples measured, 'L' is the length in between the two voltage probes, 'b' is the breadth and 't' is the sample thickness respectively.

For evaluation of polarization behaviors of the synthesized cathodes, electrical characterizations were also studied through impedance spectroscopy in the form of symmetric cells. Symmetric cells of variable configurations having variations in particulate shape and sizes of LSM were fabricated by screen printing thick paste of LSM onto opposite surfaces of dense 8YSZ discs (thicknesses ~ 1.5 mm). The screen printed layers were sintered in air at 1100 °C. The typical thicknesses of the screen printed electrodes were kept ~50 μm. Electrochemical impedance spectroscopy (EIS) measurements with the symmetric cells, thus obtained, were carried out using an impedance analyzer (Solartron 1260 A, UK) under an applied AC voltage of 100 mV in the temperature range of 600–800 °C with an increment of 50 °C in air atmosphere. The spectrum was captured for the full frequency range varied between 10^{-1} Hz and 10^{6} Hz. The impedance spectra of the cathode layers of different configurations were attempted to correlate with the particulate size and morphology of the corresponding LSM powders synthesized under different processing conditions of the present investigation.

2.3. Single cell fabrication and electrochemical testing

Anode-supported half cells with thin YSZ electrolyte layer (~ 20 μm) having configuration NiO–YSZ/YSZ were screen printed with the optimized combination of cathode functional and current collection layers having lowest polarization as envisaged from EIS spectroscopic studies and was co-fired at a temperature of 1100 °C. The details of the single cell fabrication were already reported in our earlier communication [26]. For comparison, single cells were also fabricated using CFL and CCCL using SP synthesized LSM that is devoid of any optimized particle size and morphology. The electrochemical performances of single cells [NiO–YSZ/YSZ/LSM–YSZ (CFL)/LSM (CCCL)] thus obtained, were evaluated using hydrogen (containing 3% moisture) as fuel and oxygen as oxidant at three different temperatures, viz. 700, 750 and 800 °C. The flow rates of hydrogen and oxygen were kept at 100 standard cubic centimeter per minute (SCCM). In order to study the effect of oxidant, electrochemical performance of such coupon cells were also evaluated using air as the oxidant with a flow rate of 500 SCCM. The details of the electrochemical measurement were reported in our earlier publications [26,27]. Attempt has been made to correlate the performances of single cell with the particulate size and morphology of the SP synthesized LSM. The cross sectional micrographs of single cells fabricated with conventional cathode as active and current collection layers and with SP synthesized LSM having optimized particulate size and shape were studied using a scanning electron microscopy (SEM, Leo, UK).

3. Results and discussions

3.1. Optimization of SP synthesized LSM for cathode functional (CFL) and cathode current collection (CCCL) layers based on particle size and morphology

The variations of BET surface area and the particulate diameter calculated from the surface area of the various SP synthesized LSM powders are given in Table 1. It is observed from Table 1 that, with increase in molar concentration of the precursor solution, surface area of the SP synthesized LSM powders (LS-1 to LS-4) is found to decrease systematically. Increase in molar concentration of the precursor solutions favors the volume precipitation of the solvated atomized droplet rather than the surface precipitation [28]. For substantial growth of the particulates within the reactor, precalcined ashes derived out of the precursor solution of 0.25 M (having lowest particle size of ~0.18 μm) is added to the solutions of concentrations ranging in between 0.25 and 1.0 M as tabulated in Table 1. Variation of the particulate sizes with precursor concentration with and without addition of the seeding agent is given in Fig. 2. It is vivid from the figure that addition of the seeding agent has a significant effect in the growth of the pyrolysed LSM particulates thereby enlarging the particle size and reducing the surface area. The drastic increase in the particle size of LSM powders are found to start at precursor concentration of 0.75 M having a solid loading of precalcined ashes prepared from the precursor concentration of 0.25 M. This could be attributed to the homogenous-homomolecular nucleation followed by high temperature particle growth inside the SP reactor. The critical particle sizes as obtained from Fig. 2 is ~4.8 μm corresponding to a precursor concentration of 0.87 M containing the seeding agent as the precalcined ashes derived out of precursor concentration 0.25 M. Hence, it is evident that the particle size changes systematically with the addition of seeding agent during the pyrolysis and therefore may be synthesized as desired for application in various layers in SOFC cathode.

Fig. 3a shows a typical X-ray diffractogram (for LS-1 having lowest particle size of ~0.18 μm) of the as-synthesized LSM powder prepared by spray pyrolysis. Rietveld analysis of the same shows a phase purity of about 70% without any significant amount of $LaMnO_3$ and Mn_3O_4 as secondary phases. After calcinations at 950 °C, irrespective of precursor solution concentration phase purity improves to more than 99% with the formation of a single-

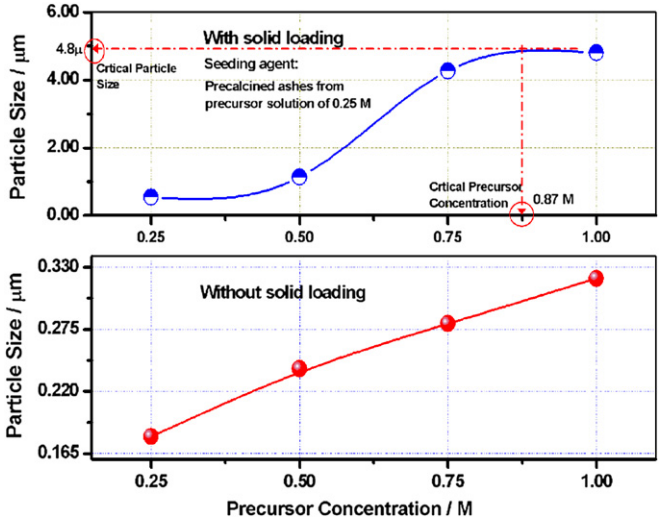

Fig. 2. Variation of particle size of SP synthesized LSM with precursor concentration and effect of solid loading.

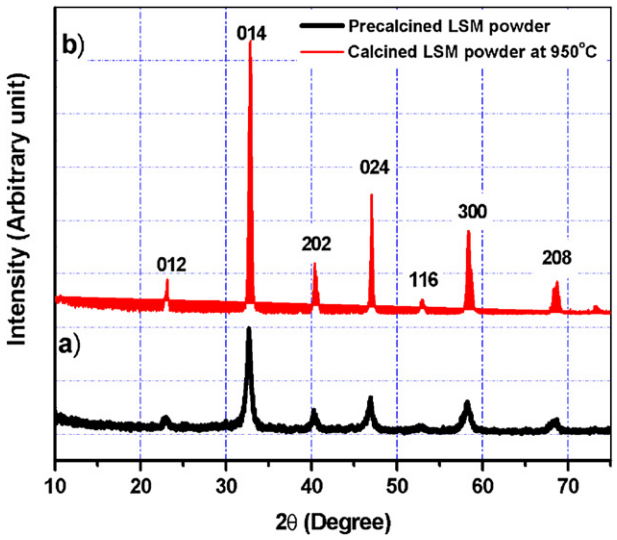

Fig. 3. Typical X-ray diffractograms of SP synthesized LS-1 composition: a) as-synthesized (pre-calcined) condition and b) calcined at 950 °C.

phase rhombohedral $La_{0.65}Sr_{0.3}MnO_3$ (Fig. 3b). The calculated lattice parameters are found to be $a = b = 5.467$Ao and $c = 13.494$Ao. The average crystallite sizes of the calcined LSM (LS-1) prepared by SP are found to be ~30 nm. It is found that the crystallite size increases with increase in precursor concentration and the highest crystallite size obtained for LS-4 is ~120 nm. The phase purity of the as-synthesized powders increases from 70 to 90% with increase in the precursor concentration from 0.25 M to 1.0 M. This may also be accredited to the fact that crystal growth is more pertinent with increase in higher heat content of the metal–ion complex gel that increases with increase in precursor concentration [28]. Increase in either crystallite size and phase purity is not observed during the particle growth upon seeding effect. This in turn indicates that upon seeding by the precalcined ashes, the particulates grow purely by homomolecular addition of primary nanoparticulates during the pyrolysis process. From Table 1 and Fig. 2, it is observed that the LS-2 having average particulate size ~0.24 μm may be utilized as the effective material applicable for SOFC cathode functional layer (CFL) because of the close proximity of the particle sizes with that of the YSZ (d_{50} = 0.22–0.25 μm). Such matching particle size is expected to enhance the triple phase boundary (TPB) for effective electrocatalytic activity to be useful for cathode application especially as CFL in SOFC application [18]. Fig. 4a shows typical FESEM micrograph that reveals the particulate morphology of such powders (LS-2) to be used as cathode functional layer (CFL). During spray pyrolysis technique, two opposite forces is operative simultaneously within the atomized droplets, viz. solvent evaporation drag and counter drag of the solute precipitation. Increased concentration of metal ion in the atomized droplet tends to accelerate the drag force exerted by solute species compared to the solvent evaporation during pyrolysis and hence results in denser spherical particulates. The solute drag is further enhanced by the addition of tiny nanoparticles into the precursor solution as seeding agents [28]. Fig. 4b shows typical morphology of micro particulates that result out of such seeding effect during SP as obtained from precursor solution of LS-1.4. It is observed that, the nanoparticles are pertinent to grow to meso and microporous particulates by nucleation and in-situ growth during such pyrolysis process. These granules having internal porosities and the primary nanoparticles embedded in the microstructure with higher particle size and reduced surface area (Table 1) are best suited to act as effective material for cathode current collection layer (CCCL). These micro particles with in-built meso and micro pores within such granules are effective for gas diffusion and may reduce the diffusion polarization for cathode layer in particular.

3.2. Electrical characterization of spray pyrolysed LSM cathode

To ascertain the aptness of the synthesized LSM powders for application as cathode functional (CFL) and current collection layer (CCCL) in SOFC, sintered bulk samples made from the selected batches viz. LS-2 and LS-1.4 are examined for DC electrical conductivity measurements using standard 4-probe technique. The details of the temperature dependent electrical conductivities along with the activation energies for electrical conduction of LS-2 and LS-1.4 samples, sintered at various temperatures (950–1150 °C), are summarized in Table 2. The corresponding Arrhenius plots, depicting the temperature dependant electrical conductivities of such samples are shown in Fig. 5. It is found that there is a strong correlation between the sintering temperature of the samples and their temperature dependent electrical conductivity. Thus, irrespective of the particulate size and morphology of the initial SP LSM, with increase in sintering temperature, the overall electrical conductivity of the sample increases. This may be attributed to the favorable sintering of the nanocrystalline SP synthesized cathodes at higher temperature. Both LS-2 and LS-1.4, exhibit similar trend of linear semiconducting type behavior within the measurement temperature range of 500–800 °C. It can be observed that the activation energy required for electrical conduction tend to alter with the variation in particle size and morphology of the LSM having identical composition (LS-2 and LS-1.4). For a particular sintering temperature, the electrical conductivity of LS-2 is found to be higher compared to that for LS-1.4. Smaller particulates having average particulate size of ~0.24 μm for LS-2 promotes sintering at a lower temperature. Consequently,

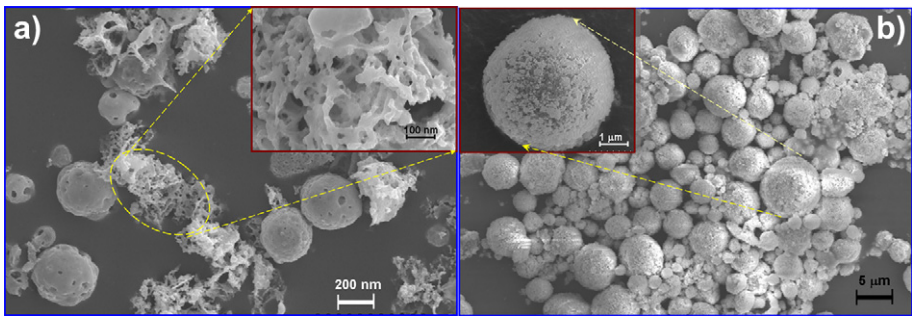

Fig. 4. Typical FESEM micrographs of: a) LS-2 utilized as cathode functional layer (CFL): *Inset – Interconnected nanoparticulates for CFL layer* and b) LS-1.4 used as cathode current collection layer (CCCL): *Inset – larger view of micron size porous granules synthesized using seeding agent during pyrolysis.*

Table 2
Electrical characteristics of SP synthesized cathode powders.

Temperature(°C)	Sintering temperature (°C)																			
	950				1000				1050				1100				1150			
	LS-2		LS-1.4		LS-2		LS-1.4		LS-2		LS-1.4		LS-2		LS-1.4		LS-2		LS-1.4	
	σ	E_a	σ	E_a	σ	E_a	σ	E_a	σ	E_a	σ	E_a	σ	E_a	σ	E_a	σ	E_a	σ	E_a
500	45	10.5	25	14.1	64	9.1	53	9.9	95	7.9	72	8.2	141	6.4	99	7.5	164	6.46	132	6.54
550	51		30		70		58		103		86		148		106		173		142	
600	56		37		75		66		116		95		157		115		187		149	
650	65		45		84		74		127		101		166		125		196		156	
700	74		57		93		83		132		109		172		134		205		164	
750	83		64		102		94		140		115		180		142		212		178	
800	92		70		115		100		152		120		195		150		228		183	

σ = Conductivity in Scm^{-1} and E_a = Activation energy in kJ mol^{-1}.

such nanometric LSM particles undergo effective sintering at 1100 °C providing much better conduction pathway so as to minimize the activation energy (E_a = 6.37 kJ mol^{-1}). Beyond a sintering temperature of 1100 °C, a marginal enhancement in energy barrier for the electrical conduction (E_a = 6.46 kJmol^{-1}) may be due to exaggerated sintering. In contrast, for the sintered samples with relatively larger LSM particulates of LS-1.4 (average particle size ~5 μm), a higher sintering temperature of 1150 °C is necessary to have an energy barrier for the electrical conduction (E_a = 6.54 kJmol^{-1}) comparable to that for the LS-2 derived samples. Thus, the highest electrical conductivity for LS-2 sintered at 1100 °C is found to be 195 Scm^{-1} at 800 °C having open porosity <2%. On the other hand, LS − 1.4 sintered at 1150 °C exhibits an electrical conductivity of 180 Scm^{-1} at the same temperature (800 °C) with open porosity of ~8%.

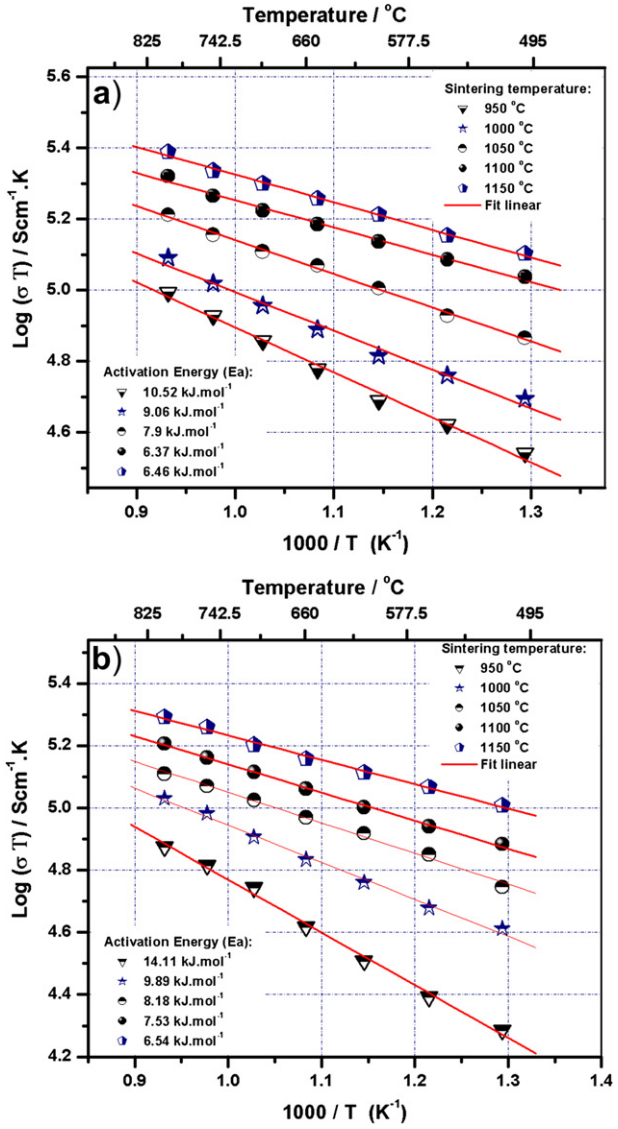

Fig. 5. Temperature dependent electrical conductivities of sintered bulk samples for SP synthesized LSM batches: a) LS-2 and b) LS-1.4.

3.3. Influence of spray pyrolysed LSM cathode on the electrochemical impedance

The effectivity of LS-2 and LS-1.4 compositions (optimized in Sections 3.1) as CFL and CCCL is studied in the present section by impedance spectroscopy. It is known that, variation in fabrication, microstructure and geometry of the associated electrodes influence the impedance spectra significantly [29–31]. Three varieties of symmetric cell are fabricated: a) Type-I, where the cathode paste consists of 1:1 mixture of LS-2 and YSZ having close proximity in particulate shape and sizes, b) Type-II, the cathode paste is comprised of a 1:1 mixture of LS-1.4 and YSZ, where significant variations are found in the particulate size, shape and porosity and c) Type-III, a bilayer composite cathode is printed with the layer wise addition of paste LS-2 + YSZ (1: 1) as the first layer and LS-1.4 as the top layer. The fabricated symmetric cells along with a characteristic impedance spectrum are shown schematically in Fig. 6a and b respectively. AC impedance study for oxygen reduction reaction (ORR) at the cathode electrode represents frequency dependent multiple phenomena wherein the rate determining step(s) could be identified and the reaction sequences can be arranged accordingly. The primary governing steps involved during ORR at cathode/electrolyte interface is written as [32]:

a) Molecular diffusion of gaseous oxygen through cathode layer
b) Adsorption of such molecular oxygen (O_2) on specific adsorption sites within cathode followed by formation of oxide (O^{2-}) ions by direct reduction or by dissociation of intermediate peroxide (O_2^{2-}) ionic species
c) Ionic diffusion of such ions through cathode and cathode/electrolyte interface involving triple phase boundary (TPB) regions
d) The ions participate with the electrode surface and involved in the transfer of charge. This charge transfer reaction (CTR) forms the basis of cathodic electrochemical reaction

The experimental impedance spectra captured in the temperature range of 700–800 °C for the symmetric cells of Type-I, Type-

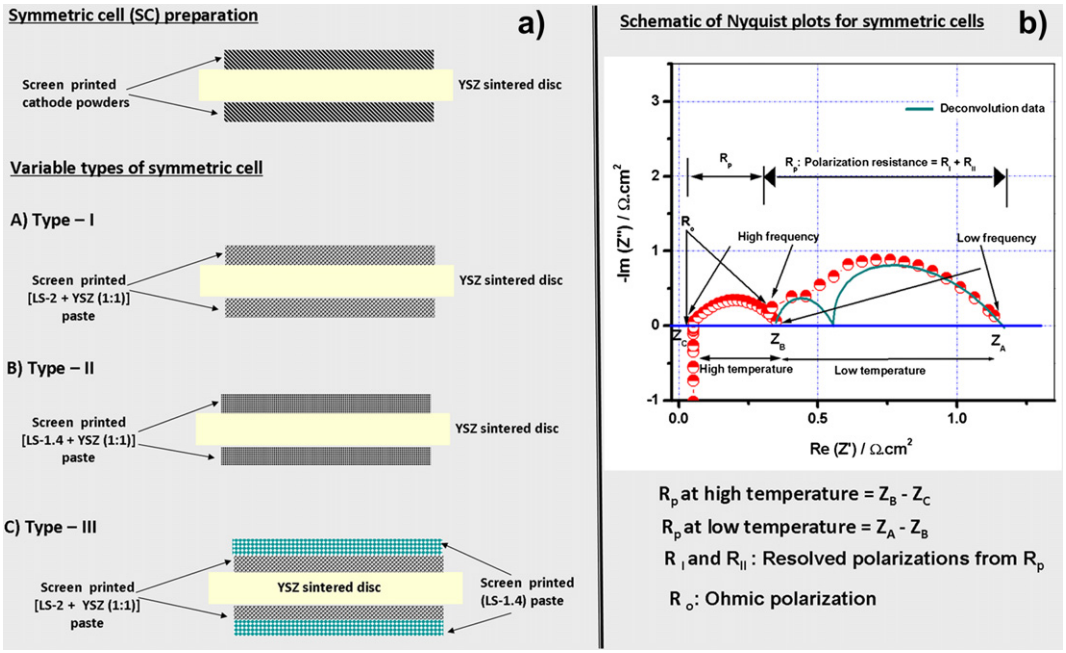

Fig. 6. a) Schematic of various types of symmetric cells fabricated with spray pyrolysed cathodes and b) Schematic of various polarizations as envisaged from Nyquist plots.

II and Type-III are shown in Fig. 7. The intercept at the real axis at high frequencies correspond to the ohmic resistance (R_o) of the cell that involves the contribution of the electrolyte. Irrespective of symmetric cell configuration, increase in operating temperature from 700 °C to 800 °C, tend to shift the position of the arc towards high frequency thereby minimizing the contribution of ohmic resistance to the overall cell. From the figure it is observed that the highest ohmic resistances of such symmetric

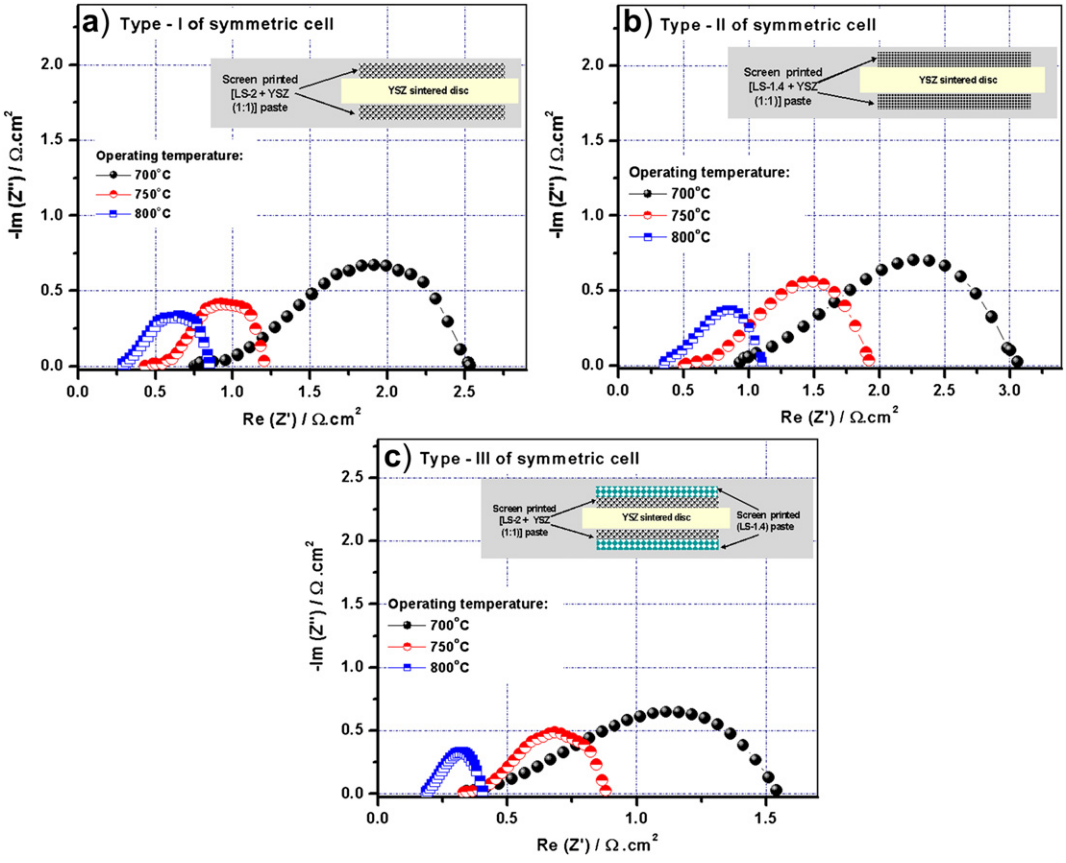

Fig. 7. AC impedance spectroscopy of fabricated symmetric cells: a) Type-I, b) Type-II and c) Type-III measured in the temperature range of 700–800 °C.

cells are found to be ~0.3 Ω-cm^2 (for Type-I), ~0.351 Ω-cm^2 (for Type-II) and the same is reduced to ~0.18 Ω-cm^2 (for Type-III) at 800 °C. The ohmic resistances for the symmetric cell of Type-III at 700 and 750 °C are found to be ~0.35 and ~0.3 Ω-cm^2 respectively. This is in agreement with the fact that the cell operation at high temperature minimizes the contribution of electrolyte resistance. Increasing the temperature from 700 to 800 °C, the overall resistance of the symmetric cell obtained from the low frequency intercepts is found to reduce from 2.53 Ω-cm^2 to 0.85 Ω-cm^2 (for Type-I), 3.06 Ω-cm^2 to 1.1 Ω-cm^2 (for Type-II) and 1.54 Ω-cm^2 to 0.405 Ω-cm^2 (for Type-III). The overall decrease in cell resistances are caused primarily by acceleration in ORR of cathode at higher temperature. The interfacial polarization resistance (R_p) of the cathode can be obtained from the difference in the magnitude of intercepts at real axis at high and low frequencies. The correlation among symmetric cell configurations and polarization resistances (R_p) at variable temperatures (600–800 °C) is given in Fig. 8a. Irrespective of the type of symmetric cell, interfacial polarization resistance holds an inverse relation with operating temperature. Such fact indisputably supports the acceleration in the rate of associated limiting steps with temperature enhancement. The associated polarization resistance of the symmetric cells of Type-III are found to be lowest compared to either Type-I or Type-II. In the low temperature region i.e. 600–700 °C, the primary resistance related to cathode polarization is offered by YSZ–YSZ interconnectivity and thereby ionic conduction is followed by the charge transfer reaction through the ion conducting phases [33]. This is reflected in Fig. 8b which shows the variation of ohmic resistance (R_o) with the temperature. The drastic drop of R_o from ~3.5 Ω-cm^2 to ~0.18 Ω-cm^2 is observed in the temperature range of 600- 800 °C for Type-III and the same is observed from ~10 Ω-cm^2 to ~0.3 Ω-cm^2 and ~16.5 Ω-cm^2 to ~0.35 Ω-cm^2 in similar temperature range for Type-I and Type-II symmetric cells respectively. The overall cathode polarization (R_p) is also dependent on the density of triple phase boundary site, dissociation of peroxide ion (O_2^{2-}) and also on the molecular diffusion [30]. The lowest value of the R_p is found to be ~0.2 Ω-cm^2 for the Type-III at 800 °C. The associated polarizations of Type-III is found to be the lowest because of the combination of the cathode current collection layer (CCCL) and cathode functional layer (CFL) having variable micro to nanoporous particulates. It is also vivid from the impedance spectra that the incorporation of CCCL reduces the diffusion polarization occurring at the lower frequency thereby enhancing the formation and dissociation of peroxide ion observed at the middle frequency range of the applied AC field [32,34]. In addition, the mutual union of CFL and CCCL tend to reduce the charge transfer polarization through proper interconnectivity between YSZ–YSZ ionic phases, diffusion polarization of molecular oxygen and polarization related to formation of oxide ion species. Such composite cathodes (Type-III) is found to be effective with a total cathode thickness of ~50 μm with individual thickness of CFL and CCCL layer as ~10 μm and ~40 μm respectively.

Nyquist plots for the symmetric cell of the three configurations are deconvoluted into two parts viz. R_I and R_{II} as shown schematically in Fig. 6b. Deconvolutions are made for measurement temperature ranging from 600 to 800 °C. Cathodic polarization is primarily governed by certain rate limiting steps which can be determined from the frequency dependent impedance spectra [35]. The high frequency semicircle arc (R_I) represents the continuity of the YSZ–YSZ phases and the electrochemical charge transfer reaction thereof. The medium and low frequency semicircle arcs (R_{II}) represents the TPB site density related to the net electrochemical reaction and molecular diffusion of oxidant at the cathode. Both the cathodic polarizations R_I and R_{II} show Arrhenius type dependence on the measurement temperatures and are shown in Fig. 9. Linear regressions determine the activation energies required for both the processes related to R_I and R_{II}. It is clear from Fig. 9a and b that, while the symmetric cell of Type-III shows the least activation energy related to both the cathodic polarizations processes viz. R_I (0.89 eV) and R_{II} (1.05 eV), Type-II exhibits the highest energy barrier for same viz. R_I (1.19 eV) and R_{II} (1.21 eV) and Type-I exhibits the intermediate range of activation energy for the above two polarization processes. These facts may be attributed to the microstructural aspects of the three types of symmetric cells fabricated under this present investigation. In Type-I symmetric cell, LSM and YSZ has the close proximity in the particulate size and LSM is found to have interconnected porosity in the nano-scale which in turn, helps in extending the overall TPB density near the cathode/electrolyte interface. This reduces the overall polarization for dissociation of oxygen to peroxide ion and its subsequent transformation to oxide ion followed by the ionic diffusion of the formed species through cathode and cathode/electrolyte interface involving TPBs. In contrast, Type-II having larger variation in particulate size and shape between LSM and YSZ results in higher cathodic polarization because of lesser effective TPB site density as well as lesser possibility of YSZ–YSZ interconnectivity. The overall cathodic polarization is found to be nominal with effective molecular diffusion for the combination of cathode layers as CFL and CCCL

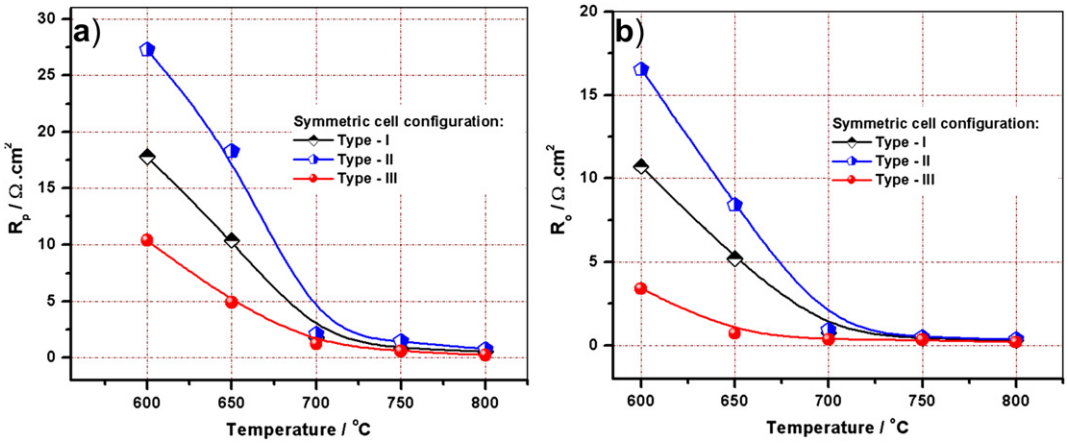

Fig. 8. Temperature dependent variation of polarization viz. a) polarization resistance (R_p) and b) ohmic resistance (R_o) for three types (I, II and III) of symmetric cells.

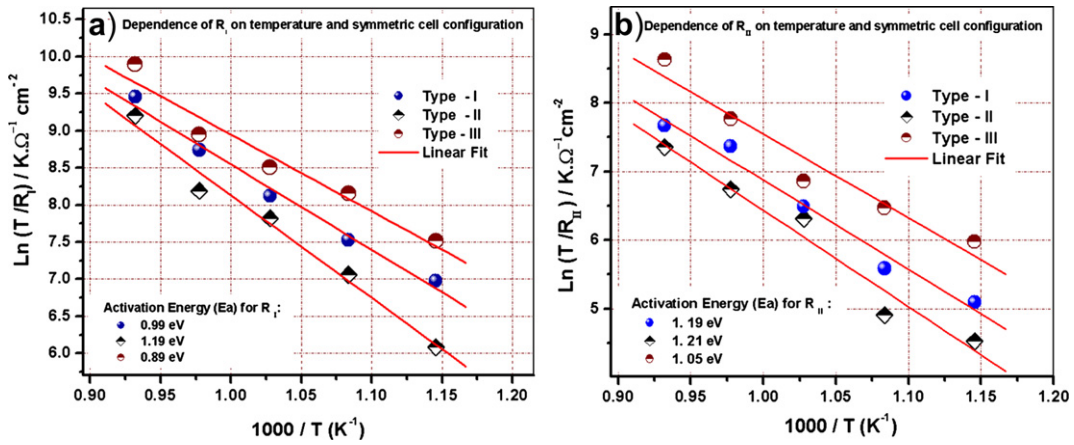

Fig. 9. Arrhenius plots for temperature dependent polarization factors resolved from cathode polarization (R_p) viz. a) R_I and b) R_{II} of the fabricated symmetric cells.

having desired particulate size and shape used in the symmetric cell of Type-III. Therefore, in the light of cathode polarizations, among the three proposed configurations of symmetric cell, the combination of CFL and CCCL of Type-III is ascertained to be best suited for SOFC cathode application.

3.4. Influence of cathode polarizations towards electrochemical activity of single cell

The polarization behavior of different cathode configurations used for symmetric cell testing, as discussed in Section 3.3, illustrates the significance of microstructural aspect of LSM particulates for their respective activities as CFL and CCCL. In the present section, the electrochemical activity of such optimized SP synthesized cathodes are discussed for SOFC application and compared with conventionally SP synthesized cathode in which particle size and morphology are not varied. Fig. 10 shows the comparative plots for the current density versus cell voltage (I–V) behavior of anode-supported single cells fabricated using different type of cathodes. Fig. 10a shows a typical performance of SOFC consisting of CFL and CCCL synthesized by conventional SP route [cell configuration: Ni–YSZ/YSZ/CFL (conventional SP synthesized LSM + YSZ)/CCCL (conventional SP synthesized LSM)]. Such cells are henceforth designated as SO-CELL-A. Fig. 10b exhibits the performance of SOFC fabricated using optimized LSM (LS-2 for CFL and LS-1.4 for CCCL) synthesized under the present investigation [cell configuration:

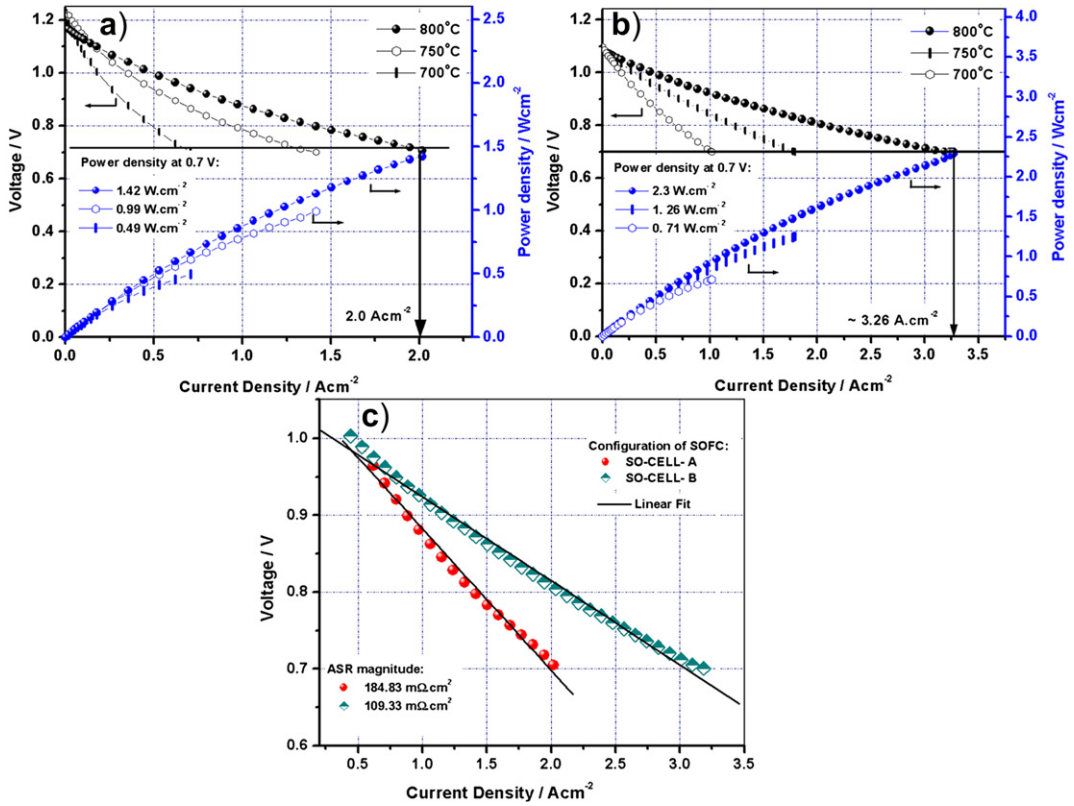

Fig. 10. Electrochemical performance of SOFC single cells at variable temperatures: a) SO-CELL-A, b) SO-CELL-B and c) area specific resistances (ASR) at 800 °C.

Table 3
Comparative electrochemical performance and ASR for single cell of varied configurations.

Single cell identification	Electrochemical performance at 0.7 V, 800 °C, A cm^{-2}		Cell area specific resistance, mΩ cm^{-2}	
	Air	Oxygen	Air	Oxygen
SO-CELL-A	1.50	2.0	225	184.8
SO-CELL-B	2.51	3.2	131	109.0

Ni–YSZ/YSZ/CFL (LS-2+YSZ)/CCCL (LS-1.4)]. Such cells are henceforth designated as SO-CELL-B. Significant enhancement in single cell performance is observed for SO-CELL-B in comparison to SO-CELL-A. Thus, at 0.7 V and 800 °C, much higher current density of 3.2 A.cm^{-2} is observed for SO-CELL-B compared to SO-CELL-A (2.0 A.cm^{-2}) under similar experimental conditions. Optimized processing conditions for synthesizing LSM (LS-2) for application as CFL enables close matching of the particulate size with that of the YSZ. The nanocrystalline particles with interconnected porosity of such synthesized LSM helps in extending the TPB length for oxygen reduction within the CFL and cathode/electrolyte junction. In-situ growth of the LSM particulates within the SP reactor helps in the formation of microporous granules of larger dimension which reduces the gas diffusion polarization and helps in current collection from the cathode surface. Furthermore, the induced functionality within SP-synthesized cathode layers (CFL and CCCL) is well justified from the reduced area specific resistance (ASR) of ∼109 mΩ cm^{-2} at 800 °C for SO-CELL-B compared to that of 184.8 mΩ cm^{-2} at 800 °C for SO-CELL-A as shown in Fig. 10c. Electrochemical testing using air as an oxidant revealed a decrease of ∼25% in the performance compared to oxygen as the oxidant. The current densities for SO-CELL-A and SO-CELL-B are found to be 1.5 A.cm^{-2} and 2.51 A.cm^{-2} at 800 °C, 0.7 V respectively with air as oxidant and hydrogen as fuel. It is found that the cell area specific resistance (ASR) of SO-CELL-A and SO-CELL -B is increased to ∼20% using air as the oxidant. The values for ASR calculated at 800 °C are found to be 225 mΩ cm^{-2} and 131 mΩ cm^{-2} using air for SO-CELL-A and SO-CELL-B respectively. The comparative electrochemical performances along with their respective ASR values are tabulated in Table 3. The reduced magnitude of ASR for SO-CELL-B is in agreement with the enhanced cell performance and minimized overall cell polarizations involving the charge transfer, ohmic and concentration polarizations. Comparative cross-sectional micrographs of single cells for SO-CELL-A and SO-CELL-B are given in Fig. 11. This explicitly describes the microstructural functionality exists in SO-CELL-B in CFL and CCCL which is responsible for such enhancement in the cell performances.

4. Conclusions

A novel spray pyrolysis (SP) technique is adopted for synthesizing doped lanthanum manganite (LSM) nanoparticulates of variable size and morphology as applicable for SOFC cathode functional layer (CFL) and cathode current collection layer (CCCL). Nanocrystalline $La_{0.65}Sr_{0.3}MnO_3$ (LSM) is synthesized with variable particulate size and morphology using precursor solutions of various concentrations to endeavor significant role towards their functionality. An attempt is made to add precalcined nanopowders synthesized from the lower concentration of the precursor solution (0.25 M) as the seeding agents to a solution having higher metal ion concentration (added quantity is 25 wt% of the theoretical yield of the precursor). This seeding is to facilitate the in-situ homogeneous-homomolecular growth of the porous nanoparticulates inside the SP reactor. SP synthesized LSM of 0.5 M concentration (LS-2) in conjunction with YSZ is found to be the best suited as cathode functional layer (CFL). Such suitability of LS-2 is not only because of the close proximity between the particle dimension of LSM (avg. particle size ∼0.24 μm) and YSZ (d_{50} ∼0.2 μm) but also because of the nanocrystalline nature of synthesized powder having interconnected porosity. It is found that in-situ growth of SP synthesized LSM initiates at ∼0.75 M precursor concentration containing precalcined ashes derived from 0.25 M precursor and reaches to saturation at a precursor concentration of 1.0 M with the same wt% of solid loading. The particulate size after significant growth is found to be ∼5 μm with a critical precursor concentration of 0.87 M. The LSM particulates thus synthesized contains primary nanoparticulates embedded within the macro granules having interconnected micro-porosity. Such unique microstructure particularly suits for effective gas diffusion and proper electrical conductivities (semiconducting) for the overall cathode current collection. The precursor of strength 0.5 M (LS-2) is found to exhibit highest electrical conductivity of 195 Scm^{-1} at 800 °C with lowest activation energy for electrical conduction (6.32 kJ mol^{-1}) after being sintered at 1100 °C. The LS-2 nanoparticulates are found to accelerate the particle sintering compared to the micron sized LSM prepared through seeding (LS-1.4). On the other hand, SP LSM micro-granules formed through particle seeding having interconnected micro porosity, functions effectively as CCCL where gas diffusion and electronic transport are the prime requisite. Detailed electrochemical impedance studies reveal that symmetric cell having CFL [LSM from 0.5 M (LS-2) + YSZ] and CCCL [LSM produced through particle seeding (LS-1.4)] exhibit lowest cathode polarization (∼0.4 Ω-cm^2) with minimum activation energy and correlated with various associated rate limiting steps. This is in agreement with the high performance of single cell (3.2 A.cm^{-2} at

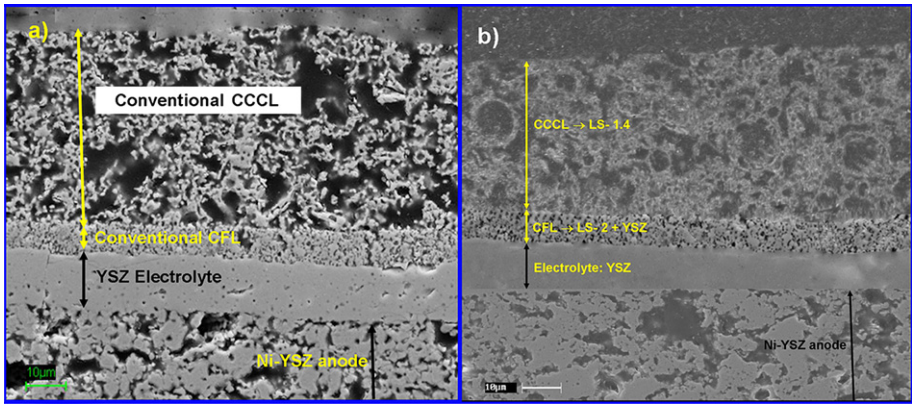

Fig. 11. Cross sectional SEM micrographs of single cell: a) SO-CELL A and b) SO-CELL B.

0.7 V and 800 °C) and lowest cell ASR (0.109 Ω-cm^2) with optimized CFL and CCCL. In contrast, single cells fabricated with CFL and CCCL prepared by conventional SP exhibit lower current density of 2.0 A.cm^{-2} (at 0.7 V and 800 °C) with lower cell ASR (0.184 Ω-cm^2). The cell performances are also correlated with their respective single cell microstructures. Therefore, appropriate particle size and morphology of nanoparticulates synthesized by optimizing the process parameters in spray pyrolysis encompass the potentiality for synthesizing multifunctional high performance SOFC cathode.

Acknowledgment

Financial support from Council of Scientific and Industrial Research (CSIR), under NMITLI Project is gratefully acknowledged. The authors are grateful to the Director of the Institute for giving permission to publish this work. The authors also acknowledge the valuable suggestions from Dr. A. Das Sharma, Senior Scientist of Fuel Cell & Battery Division, CSIR-CGCRI, Kolkata. Technical assistance rendered by Analytical Facility Division of the Institute in obtaining the XRD patterns and FESEM images of the samples is also acknowledged.

References

[1] J.P.P. Huijsmans, Curr. Opin. Solid State Mater. Sci. 5 (2001) 317–323.
[2] A. Weber, E.I. Tiffée, J. Power Sources 127 (2004) 273–283.
[3] M. Susuki, H. Sasaki, S. Otoshi, A. Kajimura, N. Sugiura, M. Ippommatsu, J. Electrochem. Soc. 141 (1994) 1928–1931.
[4] C. Sun, R. Hui, J. Roller, J. Solid State Electrochem. 14 (2010) 1125–1144.
[5] X. Sun, S. Li, J. Sun, X. Liu, B. Zhu, Int. J. Electrochem. Sci. 2 (2007) 462–468.
[6] E.I. Tiffee, Q. Weber, D. Herbstritt, J. Eur.Ceram. Soc. 21 (2001) 1805–1811.
[7] M. Mogensen, S. Skaarup, Solid State Ionics 86–88 (1996) 1151–1160.
[8] N. Grunbaum, L.S. Gallo, C. Steil, L. Dessemond, Electrochem. Soc. Trans. 25 (2009) 2367–2374.
[9] E.I. Tiffee, A. Weber, K. Schmid, V. Kerbs, Solid State Ionics 174 (2004) 223–232.
[10] M. Kuznecov, P. Otschik, P. Obenaus, K. Eichler, W. Schaffrath, Solid State Ionics 157 (2003) 371–378.
[11] R.N. Basu, F. Tietz, E. Wessel, D. Stöver, J. Mater. Process. Technol. 147 (2004) 85–89.
[12] J. Van Herle, A.J. McEvoy, K.R. Thampi, Elecrochim. Acta 39 (1994) 1675–1680.
[13] K. Sasaki, J.P. Wurth, R. Gschwend, M. Godickemeier, L.J. Gauckler, J. Electrochem. Soc. 143 (1996) 530–543.
[14] San Ping Jiang, J. Mater. Sci. 43 (2008) 6799–6833.
[15] T.Z. Sholklapper, V. Radmilovic, C.P. Jacobson, S.J. Visco, L.C. De Jonghe, Electrochem. Solid-State Lett. 10 (2007) B74–B76.
[16] T.Z. Sholklapper, H. Kurokawa, C.P. Jacobson, S.J. Visco, L.C. De Jonghe, Nano Lett. 7 (2007) 2136–2141.
[17] X. Lou, Z. Liu, S. Wang, Y. Xiu, C.P. Wong, M. Liu, J. Power Sources 195 (2010) 419–424.
[18] H.L. Tuller, Solid State Ionics 131 (2000) 143–157.
[19] K. Sato, T. Kinoshita, H. Abe, J. Power Sources 195 (2010) 4114–4118.
[20] L. Dieterle, D. Bach, R. Schneider, H. Störmer, D. Gerthsen, U. Guntow, E. Ivers-Tiffée, A. Weber, C. Peters, H. Yokokawa, J. Mater. Sci. 43 (2008) 3135–3143.
[21] N.P. Bansal, Z. Zhong, J. Power Sources 158 (2006) 148–153.
[22] A. Hagiwara, N. Hobara, K. Takizawa, K. Sato, H. Abe, M. Naito, Solid State Ionics 177 (2006) 2967–2977.
[23] J. Januschewsky, M. Ahrens, A. Opitz, F. Kubel, J. Fleig, Adv. Funct. Mater. 19 (2009) 3151–3156.
[24] B. Lai, A.C. Johnson, H. Xiong, S. Ramanathan, J. Power Sources 186 (2009) 115–122.
[25] A. Gurav, T. Kodas, T. Pluym, Y. Xiong, Aerosol Sci. Tech. 19 (1993) 411–452.
[26] R.N. Basu, A. Das Sharma, A. Dutta, J. Mukhopadhyay, Int. J. Hydrogen Energy 33 (2008) 5748–5754.
[27] A. Dutta, J. Mukhopadhyay, R.N. Basu, J. Eur. Ceram. Soc. 29 (2009) 2003–2011.
[28] G.L. Messing, S.C. Zhang, G.V. Jayanthi, J. Am. Ceram. Soc. 76 (1993) 2707–2726.
[29] R. Ahmed, K. Reifsnider, Int. J. Electrochem. Sci. 6 (2011) 1159–1174.
[30] D. Marinha, L. Dessemond, E. Djurado, J. Power Sources 197 (2012) 80–87.
[31] M. Balaguer, V.B. Vert, L. Navarrete, J.M. Serra, J. Power Sources 223 (2013) 214–220.
[32] N.Q. Minh, T. Takahashi, Science and Technology of Ceramic Fuel Cells, Elsevier, New York, USA, 1995.
[33] H.S. Song, W.H. Kim, S.H. Hyun, J. Moon, J. Kim, H.-W. Lee, J. Power Sources 167 (2007) 258–264.
[34] J. McCoppin, D. Young, T. Reitz, A. Maleszewski, S. Mukhopadhyay, J. Power Sources 196 (2011) 3761–3765.
[35] M.J. Jorgensen, M. Mogensen, J. Electrochem. Soc. 148 (2001) A433–A442.